nature photonics

Article

https://doi.org/10.1038/s41566-023-01350-6

# Observation of localization of light in linear photonic quasicrystals with diverse rotational symmetries

Received: 26 January 2023

Accepted: 16 November 2023

Published online: 4 January 2024

Check for updates

Peng Wang [1,4], Qidong Fu [1,4], Vladimir V. Konotop [2], Yaroslav V. Kartashov [3] & Fangwei Ye [1]

Since their first observation in metallic alloys, quasicrystals have remained highly intriguing ubiquitous physical structures, sharing properties of ordered and disordered media. They can be created in various ways, including optically induced or technologically fabricated structures in photonic and phononic systems. Understanding the wave propagation in such two-dimensional structures attracts considerable attention, with strikingly different localization properties observed in various quasicrystalline systems. Direct observation of localization in purely linear photonic quasicrystals remains elusive, and the impact of varying rotational symmetry on localization is yet to be understood. Here, using sets of interfering plane waves, we create photonic two-dimensional quasicrystals with different rotational symmetries. We demonstrate experimentally that linear localization of light does occur even in clean linear quasicrystals. We found that light localization occurs above a critical depth of optically induced potential and that this critical depth rapidly decreases with increasing order of the discrete rotational symmetry of the quasicrystal. These findings pave the way for achieving wave localization in a wide variety of aperiodic systems obeying discrete symmetries, with possible applications in photonics, atomic physics, acoustics and condensed matter.

Quasicrystals[1–4] are unique structures: unlike crystals, they are not periodic, that is, they do not feature translational symmetry, and at the same time, they still can continuously fill the entire space. Unlike crystals, which, by the crystallographic restriction theorem, can possess only two-, three-, four- or sixfold rotational symmetries, two-dimensional quasicrystals can feature any order of a discrete rotational symmetry, such as fivefold, sevenfold or higher symmetries (see examples in Fig. 1 below). Quasicrystalline structures—initially discovered in the process of the growth of alloys[3,4]—are nowadays extensively studied in solid-state physics[1,3–5], including twisted bilayer graphene[6,7]. They are artificially created in ultracold quantum gases[8–11], in various optoelectronic[12,13] and photonic[14–21] systems. The impact of symmetry and long-range order on wave propagation within quasicrystalline materials and structures is among the most interesting aspects under active current investigation across diverse fields.

Indeed, the evolution, transport and localization properties of waves in a given medium are determined, in particular, by its geometrical characteristics and, specifically, by its inner symmetry. For example, localization of linear excitations is impossible in homogeneous and periodic media due to their translational symmetry. At the same time, linear localization is possible in two-dimensional disordered materials[22,23]. More recently, it was predicted[24] and observed

[1]School of Physics and Astronomy, Shanghai Jiao Tong University, Shanghai, China. [2]Centro de Física Teórica e Computacional and Departamento de Física, Faculdade de Ciências, Universidade de Lisboa, Campo Grande, Portugal. [3]Institute of Spectroscopy, Russian Academy of Sciences, Moscow, Russia. [4]These authors contributed equally: Peng Wang, Qidong Fu. e-mail: fangweiye@sjtu.edu.cn

https://doi.org/10.1038/s41566-023-01350-6

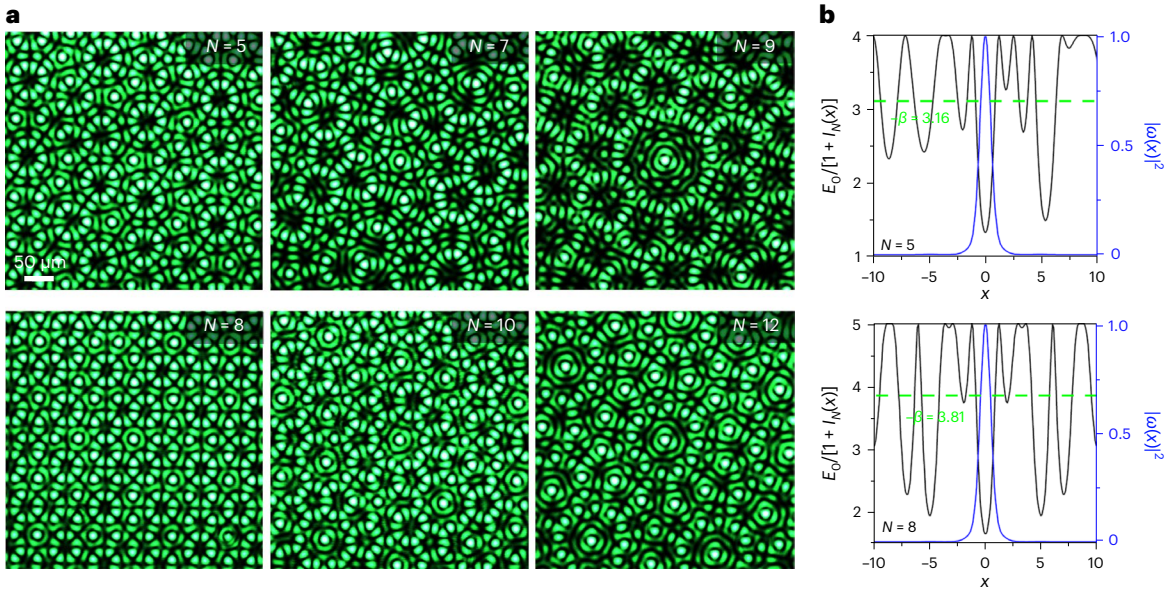


**Fig. 1 | Quasicrystals of different symmetries and cross-sections of corresponding optical potentials. a**, Experimentally generated $N$-fold symmetric quasicrystal patterns $I_N(\mathbf{r})$ with odd (upper row) and even (lower row) dihedral symmetries. The reference origin is the image centre. **b**, The representative numerically generated cross-sections of the optical quasicrystal potential $E_0/[1 + I_N(\mathbf{r})]$ for $N = 5$, $E_0 = 4$ (upper panel) and $N = 8$, $E_0 = 5$ (lower panel) along the $x$-axis at $y = 0$ of the lattice profile. The horizontal dashed green lines show the energies equal to $-\beta$ for the fundamental, most localized modes (blue curves). $\omega$ is the transverse profile of the eigenmode of the photonic quasicrystals, and $\beta$ is its propagation constant or eigenvalue. $I_N$ stands for the interference of $N$ plane waves (see its expression in the text). $E_0$ stands for the strength of the electic field.

experimentally[25] that localization of light can also occur in incommensurate moiré lattices, created by two twisted periodic sublattices and characterized by rotational point symmetry, but lacking translational symmetry. However, in all previous experimental studies of light propagation in two-dimensional quasicrystals, the localization was reported only under the action of nonlinearity[14] or additional disorder[26]. Thus, the observation of wave localization in pure quasicrystals without the action of additional confining factors remains elusive. Our work provides clear and direct experimental proof of this intriguing phenomenon by studying light propagation in reconfigurable photonic quasicrystals with various discrete symmetries, and reveals the dependence of the depth of the optical quasicrystal potential at which light localization occurs, on the order of its rotational point symmetry.

We optically induce[14] photonic quasicrystals in a photorefractive crystal of strontium barium niobate (SBN or $Sr_xBa_{1-x}Nb_2O_6$, where $x = 0.61$; dimensions = $5 \times 5 \times 20$ mm$^3$) by interfering $N$ pairs of counterpropagating coherent plane waves with transverse wavevector components $\pm\mathbf{k}_1, \pm\mathbf{k}_2, \ldots, \pm\mathbf{k}_N$, which have the same absolute values and are mutually rotated by the angles of $2\pi/N$; that is, $\mathbf{k}_j = k(\cos\theta_j, \sin\theta_j)$ with a constant $k$ and $\theta_j = 2\pi(j-1)/N$. Strontium barium niobate crystals feature a strong electro-optic anisotropy, with the electro-optic coefficient $r_{13} = 45$ pm V$^{-1}$ being much smaller than $r_{33} = 250$ pm V$^{-1}$. Accordingly, we use ordinary polarized light (affected by $r_{13}$) for the lattice induction so that the corresponding beams do not experience any noticeable self-action in the crystal, and propagate undistorted as in a uniform linear medium. By contrast, the probe light is extraordinarily polarized (affected by $r_{33}$) so it feels inhomogeneous refractive index landscape induced by the ordinary polarized beam.

In the paraxial approximation, the propagation of an extraordinarily polarized probe beam, with dimensionless amplitude $\psi(\mathbf{r}, z)$, in a photorefractive medium with an optically induced refractive index landscape, is governed by the Schrödinger equation[14]:

$$i\frac{\partial}{\partial z}\psi = H\psi, \qquad H = -\frac{1}{2}\nabla^2 + \frac{E_0}{1 + I_N(\mathbf{r})} \tag{1}$$

Here $\nabla = (\partial/\partial x, \partial/\partial y)$; $\mathbf{r} = (x, y)$ is the radius-vector in the transverse plane scaled to the wavelength $\lambda = 632.8$ nm of the beam used in the experiments; $z$ is the propagation distance scaled to the diffraction length $2\pi n_e\lambda$, where $n_e$ is the refractive index of the homogeneous crystal for extraordinarily polarized light; and $E_0 > 0$ is the dimensionless potential amplitude, controlled by bias field $E$ through $E_0 = k_0^2 n_e^4 D^2 r_{33} E/2$. Here $k_0 = 2\pi/\lambda$ is the wavenumber and $D$ is the unit of the transverse distance. The intensity of the $N$-fold symmetric optical lattice, which is induced in the sample by $N$ pairs of counterpropagating plane waves, is given by $I_N(\mathbf{r}) = [(A/N)\sum_{j=1}^{N}\cos(\mathbf{k}_j \cdot \mathbf{r} + \phi)]^2$. The non-zero stationary phase $\phi$ breaks the inversion $\mathbf{r} \to -\mathbf{r}$ symmetry, thus enabling rotational symmetries of odd orders. The amplitude of each plane wave is chosen such that the maximum of $I_N(\mathbf{r})$ and consequently the maximal depth of the lattice potential, given by $E_0/[1 + I_N(\mathbf{r})]$, remains the same for all quasicrystals used in the experiment regardless of their rotational symmetry. In our simulations, $k = 2$, $\phi = \pi/10$ and $A^2 = 2.24$. Such photonic quasicrystals obey two-dimensional dihedral symmetries $D_N$, accounting for $N$ rotations and $N$ reflections; the group properties differ for even and odd values of $N$, respectively. Restricting the consideration to non-crystalline symmetries, in Fig. 1 we show examples of the experimentally created quasicrystals with $N = 5, 7, 9$ (upper row) and $N = 8, 10, 12$ (lower row) (these patterns agree well with the numerically calculated patterns shown in Extended Data Fig. 1). The modulation of the refractive index in these experimentally created quasicrystal lattices—under the peak intensity of the writing beam, which is fixed at 40 W m$^{-2}$, and an applied electric field of $E = 300$ V mm$^{-1}$—is $\delta n = 4.4 \times 10^{-4}$.

The field of a stationary probe beam (that is, of an eigenmode) propagating in the quasicrystalline structure covering the whole transverse face of the sample is described via a solution to equation (1) of the form $\psi(\mathbf{r}, z) = w(\mathbf{r})e^{i\beta z}$, where $w(\mathbf{r})$ is the transverse profile of the mode (solving the eigenvalue problem $Hw = -\beta w$) and $\beta$ is the propagation constant. The eigenvalue problem was solved using the finite-difference method. To characterize the degree of the localization of such an eigenmode, one can use the integral form factor (alias inverse

https://doi.org/10.1038/s41566-023-01350-6

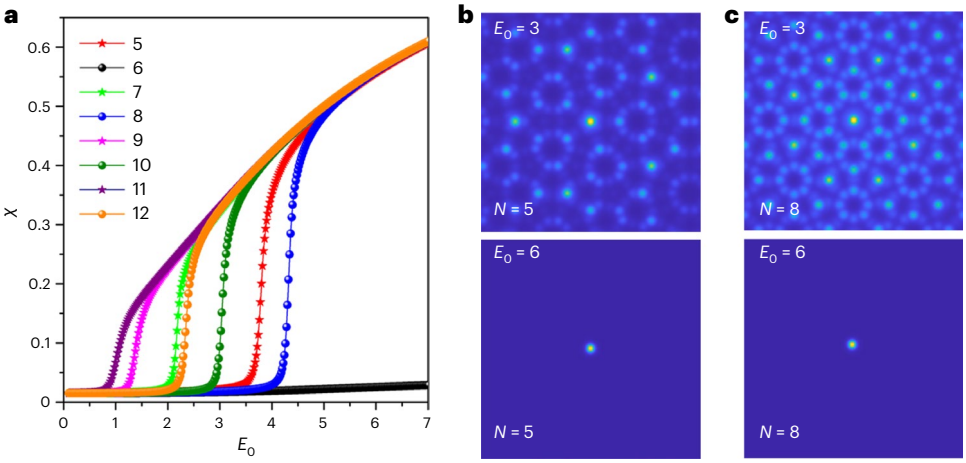


**Fig. 2 | Form factors and profiles of linear eigenmodes supported by quasicrystals. a**, The dependence of the form factor (inverse width) of the eigenmode with the largest $\beta$ on electric field $E_0$, for quasicrystals with different orders of discrete rotational symmetry $N$. For the field values $E_0$ that are well above the localization threshold, all curves $\chi(E_0)$ approach the numerically found asymptotic curve $\chi_{as} \approx -0.2138 + 0.3162\sqrt{E_0}$. The curves with stars and spheres correspond to quasicrystals with odd and even discrete rotational symmetries, respectively. **b**,**c**, Examples of the mode profiles $|w(\mathbf{r})|^2$ with the largest $\beta$ for $E_0 < E_0^{LDT}$ (upper panel) and $E_0 > E_0^{LDT}$ (lower panel) for quasicrystals with $N = 5$ (**b**) and $N = 8$ (**c**). The windows shown in **b** and **c** are $-20 \le x \le 20$ and $-20 \le y \le 20$.

participation ratio) $\chi = (\iint |\psi|^4 d^2\mathbf{r})^{1/2}/U$, where $U = \iint |\psi|^2 d^2\mathbf{r}$, with the integration over the transverse area of the quasicrystal is the energy flow. The form factor is inversely proportional to the average width of the mode: the larger the value of $\chi$, the stronger the localization. The dependence of the form factor of the most localized mode supported by the photonic quasicrystal (that is, of the mode with the largest $\beta$) on $E_0$ is shown in Fig. 2a for different values of $N$. The central result of this work is our observation that, for quasicrystals of any rotational symmetry—prohibited by the crystallographic restriction theorem—there exists a critical depth of the potential, which is defined by the applied direct current field and denoted below as $E_N^{LDT}$ (where LDT stands for the localization–delocalization transition), above which (that is, at $E_0 > E_N^{LDT}$), at least one of the guided modes becomes spatially localized, whereas at $E_0 < E_N^{LDT}$ all eigenmodes of the Hamiltonian $H$ are extended. As the transition between strongly localized and delocalized states occurs within the interval of $E_0$ values of finite widths, the critical value $E_N^{LDT}$ is defined as the point at which the respective dependence $\chi(E_0)$ changes its slope.

Within each group of odd and even order symmetries, the critical depths $E_N^{LDT}$ decrease rapidly with increasing symmetry order, that is, $E_5^{LDT} > E_7^{LDT} > \ldots$ and $E_8^{LDT} > E_{10}^{LDT} > \ldots$ (see curves marked by stars and spheres, respectively, in Fig. 2a). This separation into two sequences of symmetries corroborates with different properties of dihedral groups of odd and even orders[27]. In particular, quasicrystals obey (lack) inversion symmetry along each of the symmetry axes for even (odd) $N$, which is expected to affect light propagation. We have also found that the positions of the LDT thresholds on the energy scale correlate with the effective inhomogeneity of the refractive index, which can be characterized by the deviation of the integral refractive index at the centre of the quasicrystal from its asymptotic value on the periphery (this property can be quantified by the filling fraction $f_N$, and is investigated in Supplementary Fig. 3). For instance, we have found that the LDT threshold is a monotonically decreasing function of the filling fraction $f_N$ (Supplementary Fig. 3c). Meanwhile, for quasicrystals belonging to dihedral groups of even and odd orders, the critical depths are not strictly alternating (for example, $E_8^{LDT} > E_5^{LDT} > E_{10}^{LDT} > E_{12}^{LDT} > \ldots$). Notice that for the structure with $N = 6$, which is consistent with the crystallographic restriction theorem (that is, it is exactly periodic), no LDT is observed, all of the eigenmodes remain delocalized for any $E_0$ value that is manifested in low values of the form factor $\chi$.

We performed calculations of the density of states (DOS) in photonic quasicrystals with different symmetries to gain a better theoretical understanding of the LDT phenomenon. These calculations were conducted both above and below the LDT point, as shown in Supplementary Fig. 1. Above the LDT point, specifically for applied field $E_0 > E_N^{LDT}$, the distribution of the DOS (DOS($\beta$)) in the quasicrystals of all orders exhibits a discrete-like nature with multiple spikes and extended regions of the spectrum where the DOS is nearly zero. In this scenario, the eigenmode with the largest value of eigenvalue $\beta$ is well separated from the other modes. By contrast, below the LDT point, with applied field $E_0 < E_N^{LDT}$, the DOS($\beta$) distribution seems to be nearly continuous. In this regime, there are numerous delocalized modes that are distributed in a nearly uniform manner across the spectrum.

Yet another interesting observation is the existence of two limits in the dependencies $\chi(E_0)$ shown in Fig. 2a. The first one is a saturation limit for the form factors of the fundamental eigenmodes guided by quasicrystals of different symmetries, and this limit is well above the critical potential depth; the form factors of modes in structures with different $N$ asymptotically approach the same curve, which is well approximated by the formula $\chi_{as} \approx -0.2138 + 0.3162\sqrt{E_0}$, indicating that characteristic localization radii of the well-localized fundamental modes are practically independent of the symmetry order $N$. This independence of the form factor on the symmetry order can be explained by the isotropic properties of the central maximum of the refractive index (see Supplementary Section 1). The second limit is the minimal LDT threshold achieved at $E_0 \approx 0.4572$ when $N \to \infty$. The existence of this minimum value of LDT can be understood by observing that $\lim_{N\to\infty} I_N(r, \phi) = [AJ_0(2r)]^2$, where $J_0(\cdot)$ is the zero-order Bessel function of the first kind (see Supplementary Section 2). In this limit, the propagation problem is reduced to the existence (or non-existence) of bound states in the respective confining optical potential $-E_0[AJ_0(2r)]^2/(1 + [AJ_0(2r)]^2)$, which tends to zero at $r \to \infty$. However, this decay is very slow and the known results[28,29] on the existence of at least one bound state at any $E_0$, are not applicable to it. Instead, in Supplementary Section 2, we show that for small enough $E_0$, such potential cannot sustain guided modes, that is, guidance can be enabled only by the bias fields of finite amplitudes.

We emphasize that localized eigenmodes reported here are not defect modes, which one may expect to find in deep potential minima; by contrast, these states are enabled by interference. To illustrate this, in Fig. 1b we show representative profiles of the localized fundamental modes and their energies $-\beta$ (green dashed lines) with respect to the

https://doi.org/10.1038/s41566-023-01350-6

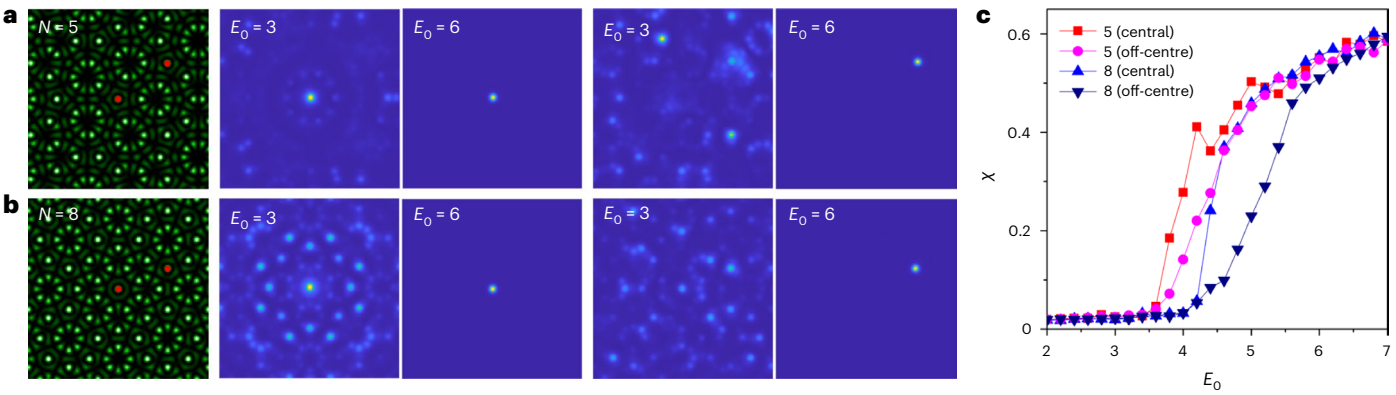


**Fig. 3 | Propagation of input Gaussian beams and their form factors.** **a**,**b**, Simulated propagation of an input Gaussian beam in fivefold (**a**) and eightfold (**b**) symmetric quasicrystals. The red dots in the lattice images in **a** ($N = 5$) and **b** ($N = 8$) indicate the location of the central and off-centre Gaussian excitations. The second and third columns show the corresponding output intensity distributions, after propagation distance $z = 50$ cm, in the quasicrystal for central excitation, whereas the fourth and fifth columns are for off-centre excitation. The windows shown in **a** and **b** are $-20 \le x, y \le 20$. **c**, Form factor of the output light field extracted from the propagation simulation at a distance $z = 50$ cm versus $E_0$ for both central and off-centre input beams.

optical potential. One observes that for both $N = 5$ and $N = 8$ structures, the $-\beta$ energy level crosses multiple local potential minima (behaviour that clearly contrasts with that of the defect modes), but the fundamental modes remain strongly localized in the vicinity of the central minimum and do not undergo diffraction due to tunnelling to the nearest local minima.

In Fig. 2b,c we compare the profiles of the fundamental modes in the quasicrystals, where $E_5^{\mathrm{LDT}} \approx 3.6$ for $N = 5$, and $E_8^{\mathrm{LDT}} \approx 4.1$ for $N = 8$, for potential depths below and above respective $E_N^{\mathrm{LDT}}$. The modes for $E_0 = 3 < E_{5,8}^{\mathrm{LDT}}$ are delocalized (only central regions are shown in Fig. 2b,c, whereas the actual calculation window is much larger), whereas the modes at $E_0 = 6 > E_{5,8}^{\mathrm{LDT}}$ are localized practically on one central spot of the potential. This is the case for all quasicrystal lattices with $E_0$ values well above the critical depth, as form factors of fundamental modes in this limit approach practically the same value $\chi_{\mathrm{as}}(E_0)$.

Simulations of direct propagation within the framework of equation (1)—using the split-step fast Fourier-transform method with an input Gaussian beam $\psi(\mathbf{r}, 0) = \exp(-|\mathbf{r}|^2/r_0^2)$ of width $r_0 = 1$, which covers roughly one local maximum of the induced quasicrystal lattice—are reported in second and third columns of Fig. 3a,b. As predicted by the analysis of the eigenvalue problem $Hw = -\beta w$, for $E_0 < E_N^{\mathrm{LDT}}$, the beam quickly diffracts (second column of Fig. 3a,b), whereas for $E_0$ above $E_N^{\mathrm{LDT}}$, the beam remains well-localized at all distances (third column of Fig. 3a,b). Importantly, this observation does not depend on the position of the initial Gaussian excitation at the input face of the crystal. Namely, for the off-centre incidence described by $\psi(\mathbf{r} - \mathbf{r}_{\mathrm{in}})$ ($\mathbf{r}_{\mathrm{in}} = 11.3\mathbf{i} + 8.1\mathbf{j}$ in Fig. 3a, and $\mathbf{r}_{\mathrm{in}} = 11.1\mathbf{i} + 4.6\mathbf{j}$ in Fig. 3b; they were chosen to be one of the $N$ local maxima on a ring of a certain radius in the lattice; see Supplementary Fig. 4 for an illustration), the beam also shows diffraction or localization depending on whether the $E_0$ value is below or above the critical value $E_N^{\mathrm{LDT}}$ (see columns four and five in Fig. 3a,b), just as for the central excitation. Indeed, the integral form factor $\chi$, calculated at the distance $z = 500$ (corresponding to a physical distance $z = 50$ cm), illustrates that the LDT value $E_N^{\mathrm{LDT}}$ is practically the same for the central and off-centre excitations (Fig. 3c; see Supplementary Figs. 2 and 4 for more off-centre excitation results).

For the experimental observation of light localization, we first employ representative members of the photonic quasicrystals family, with odd $N = 5$ and even $N = 8$ discrete rotational symmetries (Fig. 4a). To probe light propagation in them, an extraordinarily polarized signal beam was focused on the input facet of the quasicrystal lattice. The signal beam was about 22 μm in diameter and coupled into a selected local refractive index maximum of the quasicrystal. The selected local maximum can be located in the rotational centre of the quasicrystal, or it can be launched at the off-centre position, as individually indicated with the red dots in Fig. 4a. To ensure that the input beam does not distort the induced refractive index profile and that it propagates in the crystal in the linear regime, the bias field was turned off after the lattice was prepared, and the power of signal beam was taken approximately 10 nW—nearly $10^3$ times lower than the power of the lattice-creating beam.

Experimental evidence of the light localization in quasicrystals for both central and off-centre excitation conditions is presented in Fig. 4, in which we compare output patterns for the probe beam after propagation through the fivefold ($N = 5$) and eightfold ($N = 8$) symmetric 2-cm-long quasicrystals for different applied electric fields $E$ (see Extended Data Fig. 2 for more results on quasicrystal lattices with other $N$). As shown in Fig. 4b,c, for a fixed $N$, a relatively sharp LDT occurs when $E$ exceeds a certain critical value $E_N^{\mathrm{LDT}}$, indicating a clear transition from the beam diffraction to spatial localization. In the experiment we measured $E_5^{\mathrm{LDT}} \approx 300$ V mm$^{-1}$ and $E_8^{\mathrm{LDT}} \approx 360$ V mm$^{-1}$ for quasicrystals featuring five and eightfold rotational symmetries, respectively. Thus, as compared in Fig. 4b,c, when $E < E_N^{\mathrm{LDT}}$, the light in the quasicrystal lattices notably diffracts upon propagation and expands across multiple local maxima in the vicinity of the excitation point. When $E > E_N^{\mathrm{LDT}}$, diffraction is clearly arrested and a localized spot is observed at the output. As predicted by the numerical analysis and confirmed here experimentally, the critical applied field $E_N^{\mathrm{LDT}}$ is nearly the same for the central and off-centre excitation conditions (Fig. 4d).

It is important to note that the experimentally observed localizations in quasicrystal lattices are due to the interference effect, that is, they are determined by global, rather than local, symmetry properties of the underlying structures. To confirm that no additional disorder or defects were introduced into our optically induced quasicrystal lattices, which could lead to light localization, we conducted a comparison experiment in the commensurate case ($N = 6$) for which the optically induced structure is exactly periodic. In this case, we observed substantial diffraction of light for any position of the probe beam (Extended Data Fig. 2). As we used the same set-up and method to induce all quasicrystal lattices for varying $N$ (they differ only in the employed phase masks), this ensures that disorder and defects are absent in the lattices for any other $N$ values. Besides, to ensure the reproducibility of the results and to eliminate the possible influence of any anisotropy in the response of photorefractive crystals, we performed the experiments five times for each $N$ value. Before each experiment, the previously created structures were erased, and the quasicrystal lattice was rewritten to a different location across the sample (this was achieved

https://doi.org/10.1038/s41566-023-01350-6

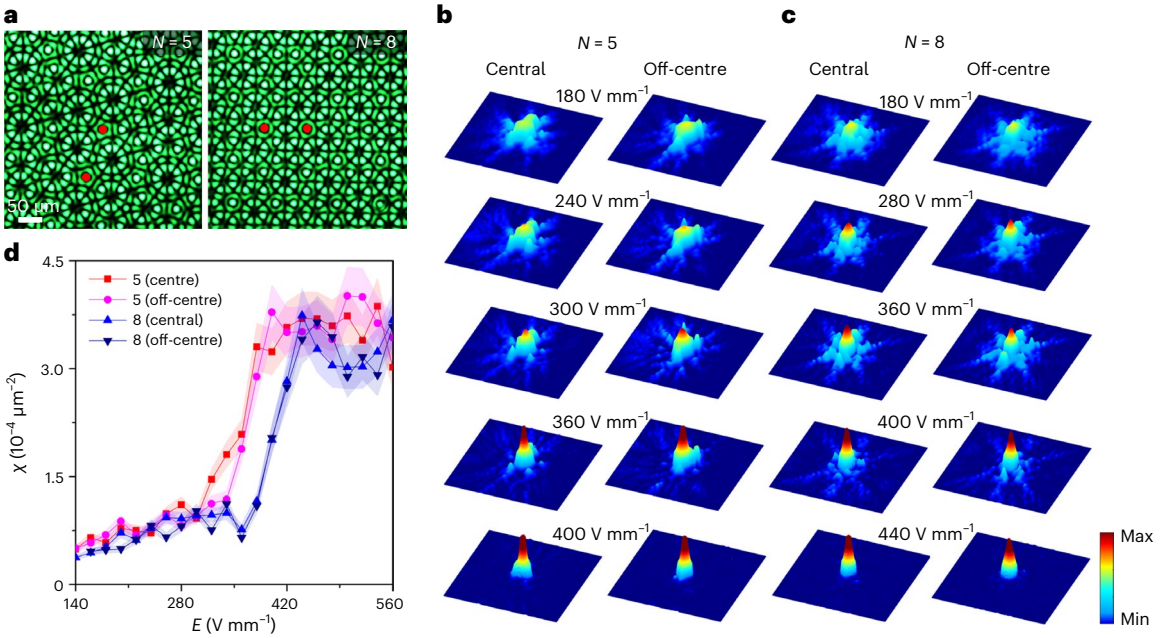


**Fig. 4 | Experimental observation of light localization in quasicrystals.** **a**, Experimentally realized quasicrystal lattices with $N = 5$ and $N = 8$. The red dots indicate the locations where the probe beam is launched. **b**, Observed output intensity distributions of probe beam after propagating in quasicrystal lattices with $N = 5$, illustrating LDT with increasing applied electric field for both central and off-centre excitations. **c**, The same as **b** but for quasicrystals with $N = 8$. The applied field $E$, measured in V mm$^{-1}$, is indicated between the respective output profiles. In **b** and **c**, the distributions are shown within a 400 μm × 400 μm window. **d**, Experimentally measured form factor at the output facet of the quasicrystal versus applied field for central and off-centre excitations. The shaded areas represent the uncertainties of the form factor introduced during the lattice creation and signal beam measurement.

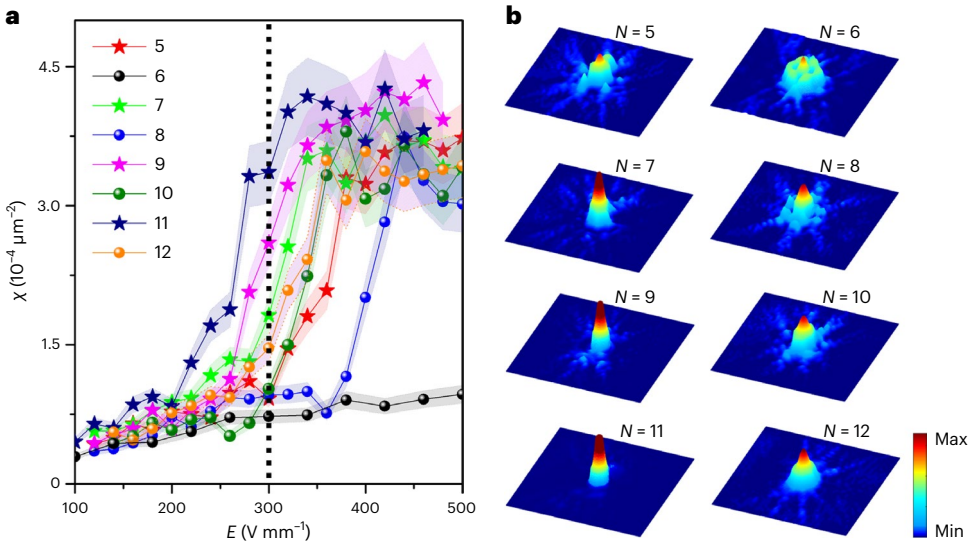


**Fig. 5 | Experimental results for different orders of the point rotational symmetry of the quasicrystals. a**,**b**, Experimentally measured form factor versus applied field (**a**), and the observed output intensity distributions for the probe beam at $E = 300$ V mm$^{-1}$ (indicated by the vertical dotted line in **a**) (**b**) for quasicrystal lattices with $N$ increasing from 5 to 12. Central excitation is used in all of the cases shown here. The shaded areas in **a** represent the uncertainties of the form factor; in **b** the distributions are shown within a 400 μm × 400 μm window.

by displacement of the mask; see Methods). We then repeated measurements of the output patterns. Therefore, each point in Fig. 4d and Fig. 5a represents the average of five measurements, and this guarantees that any possible disorder of defects are ruled out as factors affecting localization in specific realizations of the lattice.

Finally, we experimentally study the impact of the symmetry order $N$ of the quasicrystal on the light localization by comparing the respective form factors $\chi$ for the output probe beams versus $E$, for $N$ increasing from $N = 5$ to 12. As shown in Fig. 5a, for all orders of discrete rotational symmetry of the crystal, except $N = 6$ (which corresponds to the periodic lattice), the dependence of $\chi$ on $E$ exhibits a clear jump from lower to higher values after undergoing a rather narrow transition regime, and the transition point clearly decreases with increasing $N$ (if one considers odd and even values of $N$ separately), which is in good agreement with the numerical results presented in Fig. 2. As one can see, the experimental measurements reveal saturation of the form factor around $E = 400$ V mm$^{-1}$, where we estimate the induced refractive index to be $\delta n = 5.87 \times 10^{-4}$. In Fig. 5b, the output intensity distributions

are presented for quasicrystals with different rotational point symmetries at the fixed electric field $E = 300\ \mathrm{V\ mm^{-1}}$, which is substantially lower than the critical field $E_5^{\mathrm{LDT}}$ for a fivefold-symmetric quasicrystal. Accordingly, for $N = 5$, the probe beam experiences notable diffraction following propagation; diffraction is also observed for $N = 8, 10$ and 12. For quasicrystals with $N = 7$, the electric field is near the critical value at which the transition to localization occurs, and so the tendency to suppress diffraction is obvious. Finally, for crystals with $N = 9$ or 11, the selected electric field is larger than the critical value, and one observes well-pronounced localization on the entire length of the sample. Note that, in our experiment, the use of the translation stage with a mounted charge-coupled device camera (Extended Data Fig. 3) allows recording of the light intensity at every distance $z$ inside of the sample. Meanwhile, our experimental results do not reproduce the law $\chi_{\mathrm{as}}(E_0)$, shown in Fig. 2a. Instead, the increase in $E_0$ results in the saturation of $\chi$ to a constant. We attribute this disagreement of the numerical and experimental asymptotic behaviours to the fact that the crystal cannot provide an indefinitely high refractive index contrast: nonlinear effects start playing the role at sufficiently strong values of the field $E_0$.

In conclusion, we reported an investigation and observation of the impact of discrete rotational symmetry on the LDT in a photonic quasicrystal. By continuously tuning parameters, we found that the critical depth of quasicrystals controlling the LDT decreases with increasing order of the discrete rotational symmetry. The observation reported in this work clarifies fundamental aspects of the evolution of linear excitations in wave systems with quasicrystal structure and may shed light on the explanation of localization phenomena in aperiodic photonic crystals and photonic crystal fibres, phononic systems, and Bose–Einstein condensates held in optically induced quasicrystal lattices[30–32]. The phenomenon of light localization in quasicrystals may be employed for the design of micro-lasers without the need for conventional laser cavity[33], may be used to enhance the nonlinear parametric interactions of light waves[34], and in cavity quantum electrodynamics.

## Online content

Any methods, additional references, Nature Portfolio reporting summaries, source data, extended data, supplementary information, acknowledgements, peer review information; details of author contributions and competing interests; and statements of data and code availability are available at https://doi.org/10.1038/s41566-023-01350-6.

## References


1. Shechtman, D., Blech, I., Gratias, D. & Cahn, J. W. Metallic phase with long-range orientational order and no translational symmetry. *Phys. Rev. Lett.* **53**, 1951 (1984).
2. Levine, D. & Steinhardt, P. J. Quasicrystals: a new class of ordered structures. *Phys. Rev. Lett.* **53**, 2477 (1984).
3. Steurer, W. Quasicrystals: What do we know? What do we want to know? What can we know? *Acta Crystallogr. A* **74**, 1–11 (2018).
4. Steurer, W. Twenty years of structure research on quasicrystals. Part I. Pentagonal, octagonal, decagonal and dodecagonal quasicrystals. *Z. Kristallogr. Cryst. Mater.* **219**, 391–446 (2004).
5. Kamiya, K. et al. Discovery of superconductivity in quasicrystal. *Nat. Commun.* **9**, 1–8 (2018).
6. Ahn, S. J. et al. Dirac electrons in a dodecagonal graphene quasicrystal. *Science* **361**, 782–786 (2018).
7. Yao, W. et al. Quasicrystalline 30° twisted bilayer graphene as an incommensurate superlattice with strong interlayer coupling. *Proc. Natl Acad. Sci. USA* **115**, 6928–6933 (2018).
8. Sbroscia, M. et al. Observing localization in a 2D quasicrystalline optical lattice. *Phys. Rev. Lett.* **125**, 200604 (2020).
9. Mace, N., Jagannathan, A. & Duneau, M. Quantum simulation of a 2D quasicrystal with cold atoms. *Crystals* **6**, 124 (2016).
10. Lellouch, S. & Sanchez-Palencia, L. Localization transition in weakly interacting Bose super-fluids in one-dimensional quasiperiodic lattices. *Phys. Rev. A* **90**, 061602(R) (2014).
11. Sanchez-Palencia, L. & Lewenstein, M. Disordered quantum gases under control. *Nat. Phys.* **6**, 87–95 (2010).
12. Tanese, D. et al. Fractal energy spectrum of a polariton gas in a Fibonacci quasiperiodic potential. *Phys. Rev. Lett.* **112**, 146404 (2014).
13. Goblot, V. et al. Emergence of criticality through a cascade of delocalization transitions in quasiperiodic chains. *Nat. Phys.* **16**, 832–836 (2020).
14. Freedman, B. et al. Wave and defect dynamics in nonlinear photonic quasicrystals. *Nature* **440**, 1166–1169 (2006).
15. Chan, Y. S., Chan, C. T. & Liu, Z. Y. Photonic band gaps in two dimensional photonic quasicrystals. *Phys. Rev. Lett.* **80**, 956 (1998).
16. Freedman, B., Lifshitz, R., Fleischer, J. W. & Segev, M. Phason dynamics in nonlinear photonic quasicrystals. *Nat. Mater.* **6**, 776–781 (2007).
17. Xavier, J., Boguslawski, M., Rose, P., Joseph, J. & Denz, C. Reconfigurable optically induced quasicrystallographic three-dimensional complex nonlinear photonic lattice structures. *Adv. Mater.* **22**, 356–360 (2010).
18. Boguslawski, M., Rose, P. & Denz, C. Increasing the structural variety of discrete nondiffracting wave fields. *Phys. Rev. A* **84**, 013832 (2011).
19. Vardeny, Z. V., Nahata, A. & Agrawal, A. Optics of photonic quasicrystals. *Nat. Photon.* **7**, 177–187 (2013).
20. Steurer, W. & Sutter-Widmer, D. Photonic and phononic quasicrystals. *J. Phys. D* **40**, R229 (2007).
21. Guidoni, L., Trich´e, C., Verkerk, P. & Grynberg, G. Quasiperiodic optical lattices. *Phys. Rev. Lett.* **79**, 3363 (1997).
22. Wiersma, D. S. Disordered photonics. *Nat. Photon.* **7**, 188–196 (2013).
23. Segev, M., Silberberg, Y. & Christodoulides, D. N. Anderson localization of light. *Nat. Photon.* **7**, 197–204 (2013).
24. Huang, C. et al. Localization–delocalization wavepacket transition in Pythagorean aperiodic potentials. *Sci Rep.* **6**, 32546 (2016).
25. Wang, P. et al. Localization and delocalization of light in photonic moiré lattices. *Nature* **557**, 42–46 (2020).
26. Levi, L. et al. Disorder-enhanced transport in photonic quasicrystals. *Science* **332**, 1541–1544 (2011).
27. Cameron, P. G. *Introduction to Algebra* (Oxford Univ. Press, 1998).
28. Landau, L. D. & Lifshitz, E. M. *Quantum Mechanics (Non-relativistic Theory)* (Butterworth-Heinemann, 1981).
29. Simon, B. The Bound state of weakly coupled Schrödinger operators in one and two dimensions. *Ann. Phys.* **97**, 279 (1976).
30. Sanchez-Palencia, L. & Santos, L. Bose–Einstein condensates in optical quasicrystal lattices. *Phys. Rev. A* **72**, 053607 (2005).
31. Viebahn, K., Sbroscia, M., Carter, E., Yu, J.-C. & Schneider, U. Matter-wave diffraction from a quasicrystalline optical lattice. *Phys. Rev. Lett.* **122**, 110404 (2019).
32. Gautier, R., Yao, H. & Sanchez-Palencia, L. Strongly interacting bosons in a two-dimensional quasicrystal lattice. *Phys. Rev. Lett.* **126**, 110401 (2021).
33. Mao, X., Shao, Z., Luan, H., Wang, S. & Ma, R. Magic-angle lasers in nanostructured moiré superlattice. *Nat. Nanotechnol.* **16**, 1099 (2021).
34. Huang, L., Zhang, W. & Zhang, X. Moiré quasibound states in the continuum. *Phys. Rev. Lett.* **128**, 253901 (2022).

## Methods

### Experimental set-up

The experimental set-up is sketched in Extended Data Fig. 3. We used the technique of computer-generated holography to produce the desired quasicrystal lattice. Initially, the phase information of the targeted lattice, which corresponds to the interference wave field of $N$ pairs of counterpropagating plane waves, was encoded into a phase-only spatial light modulator (SLM) that had a resolution of 1,920 × 1,200 pixels controlled by a computer. An example phase diagram ($N = 5$) encoded into the SLM is presented in the inset of Extended Data Fig. 3, and more diagrams are presented in Supplementary Fig. 5. The interference wave field was then reconstructed by illuminating the SLM with a continuous-wave laser with $\lambda = 532$ nm and ordinary polarization. It should be noted that, although the reconstructed wave field seems to be visually similar to the target quasicrystal lattices, it cannot be directly written into the SBN crystal as it does not form a well-non-diffracting light beam. To overcome this limitation, we converted the wave field into the wavevector domain, filtered out any unwanted components (using a Fourier Mask placed at the Fourier plane of the 4$f$ optical system, which allowed only the first-order diffraction pattern to pass), and then transformed it back to the space domain. This process ensures the creation of a smooth and well-nondiffracting wave field throughout the 2 cm long of sample.

A signal light with wavelength 633 nm and extraordinary polarization was used to probe the propagation dynamics of light in photonic quasicrystal lattices. A translation stage equipped with a charge-coupled device camera was used to record the intensity distribution of the probe beam at different locations inside of the sample, after the lattice behind each respective location was erased.

In our experiments involving off-centre excitations, we selected one of the $N$ local maxima on a ring with a certain radius in the lattice as the excitation point. We usually chose any of the $N$ local lattice maxima on the first, second or third rings with radii ranging from tens to a few hundreds of micrometres. As the input probe beam has a diameter of approximately 22 μm, while the sample has a transverse dimension 5 mm × 5 mm, we made sure that the selected excitation points were sufficiently far away from the boundaries of the finite-size structure. As a result, the impact of the boundary effects can be safely ignored.

## Data availability

The data that support the findings of this study are available from the corresponding author on reasonable request.

## Code availability

The codes that support the findings of this study are available from the corresponding author on reasonable request.

## Acknowledgements

P.W., Q.F. and F.Y. acknowledge the support of "Shanghai Jiao Tong University Scientific and Technological Innovation Funds", and Shanghai Outstanding Academic Leaders Plan (grant no. 20XD1402000). P.W. acknowledges funding from the National Natural Science Foundation (grant no. 12304366) and China Postdoctoral Science Foundation (grant no. BX20230217). Q.F. acknowledges the support of China Postdoctoral Science Foundation (grant no. BX20230218). V.V.K. acknowledges financial support from the Portuguese Foundation for Science and Technology (FCT) under Contracts PTDC/FIS-OUT/3882/2020 and UIDB/00618/2020. Y.V.K. acknowledges funding by the research project no. FFUU-2021-0003 of the Institute of Spectroscopy of the Russian Academy of Sciences. We would like to express our gratitude to the anonymous referees for their valuable suggestions regarding the filling fractions and structure factors used to elucidate the order of the quasicrystals in explaining the threshold LDT.

## Author contributions

All of the authors susbtantially contributed to the paper.

## Competing interests

The authors declare no competing interests.

## Additional information

**Extended data** is available for this paper at https://doi.org/10.1038/s41566-023-01350-6.

**Supplementary information** The online version contains supplementary material available at https://doi.org/10.1038/s41566-023-01350-6.

**Correspondence and requests for materials** should be addressed to Fangwei Ye.

**Peer review information** *Nature Photonics* thanks Gianluigi Zito and the other, anonymous, reviewer(s) for their contribution to the peer review of this work.

https://doi.org/10.1038/s41566-023-01350-6

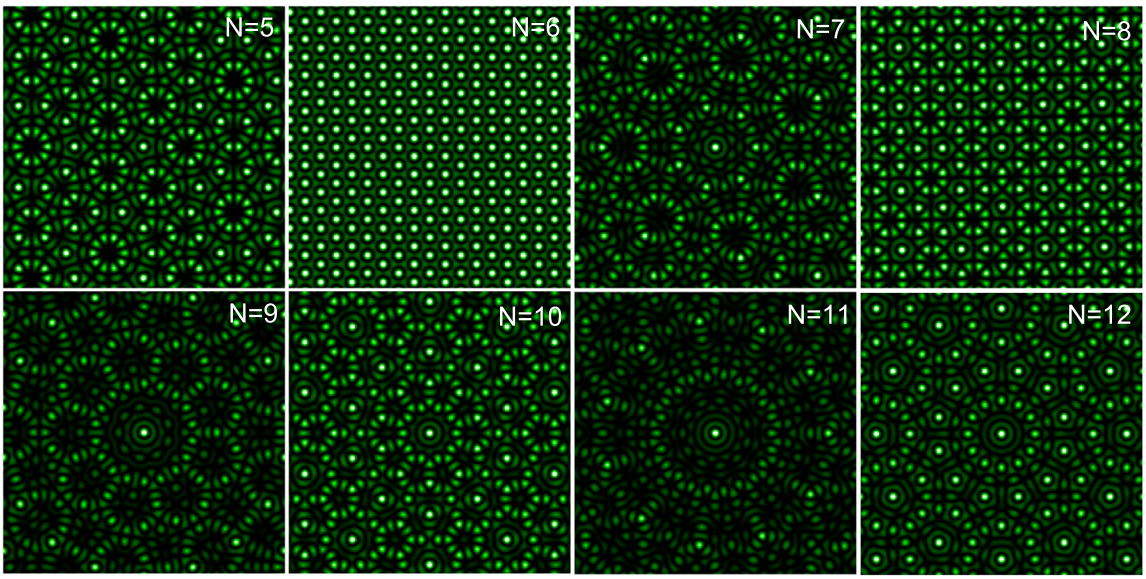


**Extended Data Fig. 1 | Numerically calculated symmetric quasicrystal patterns.** Numerically calculated N-fold symmetric quasicrystal patterns with N = 5, 7, 8., 12, as well as the periodic pattern with N = 6, for k = 2 and $A^2 = 2.24$.

https://doi.org/10.1038/s41566-023-01350-6

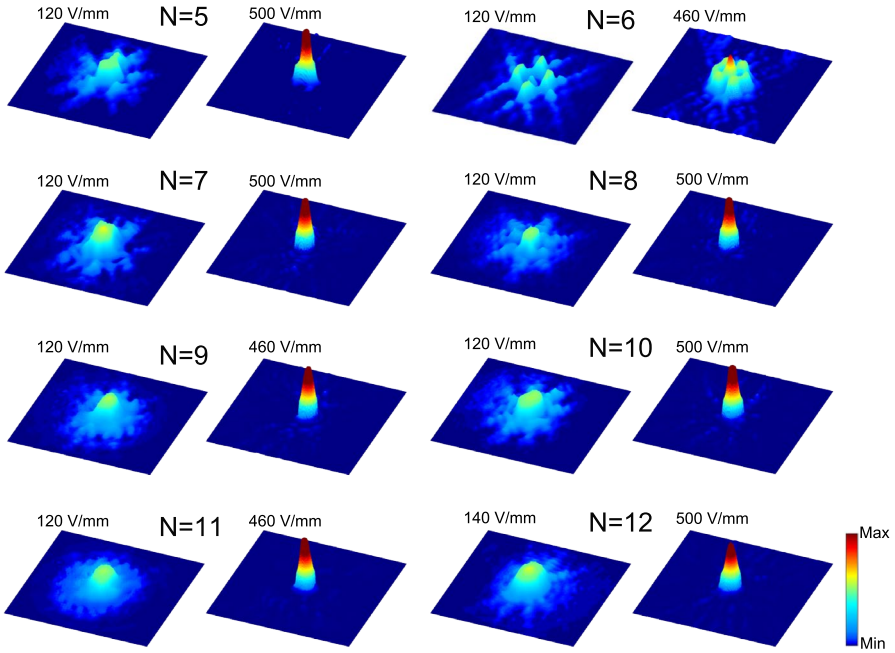


**Extended Data Fig. 2 | Experimentally intensity distributions below and above LDT point.** Experimentally observed delocalized output intensity distributions for probe beam observed below LDT point (at low values of the applied electric field) and localized distributions observed above LDT point (at sufficiently high values of the electric field), for N = 5, 7-12. At N = 6 the field is delocalized at all amplitudes of the electric field. The distributions are shown within the window of 400 μm × 400 μm.

https://doi.org/10.1038/s41566-023-01350-6

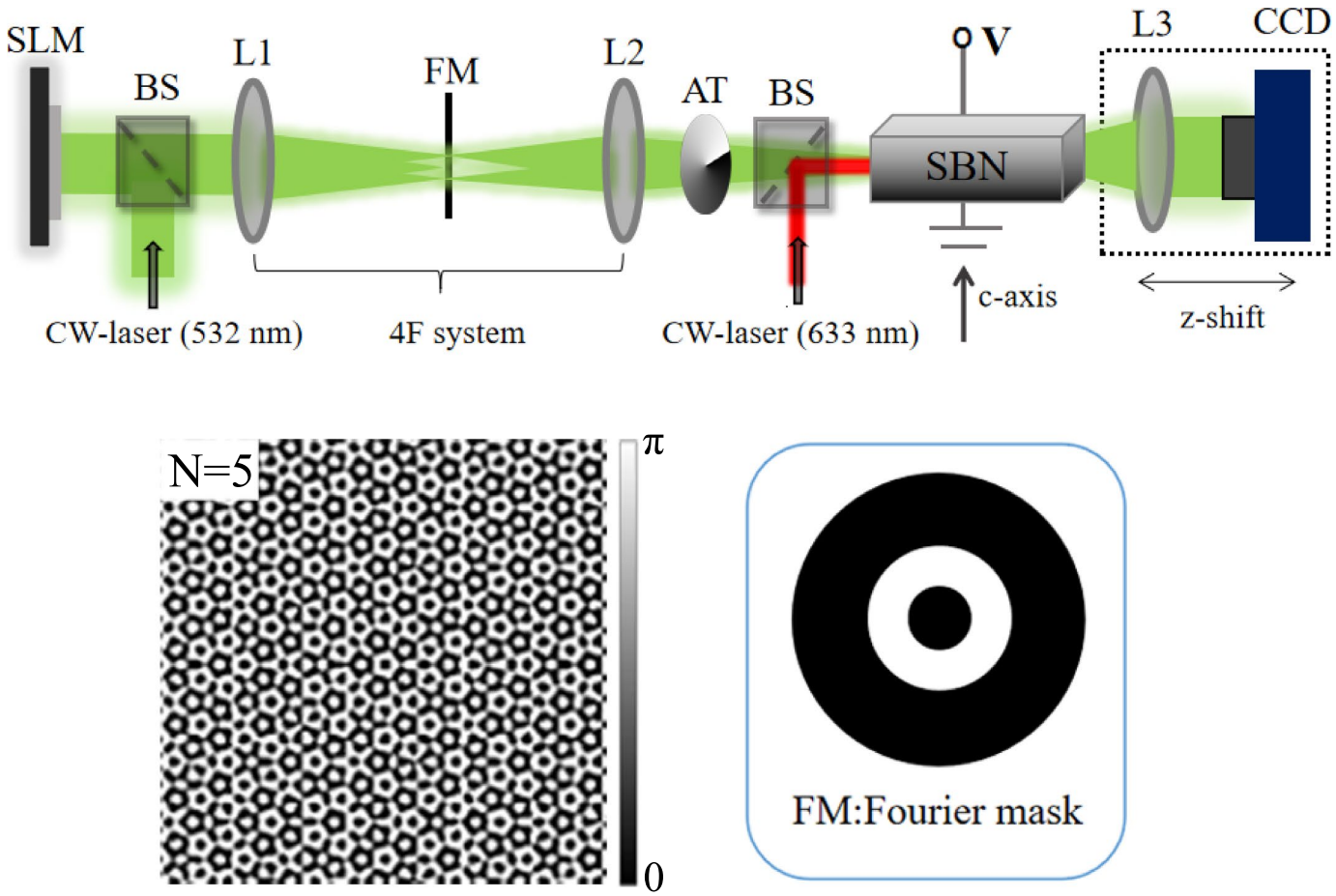


**Extended Data Fig. 3 | Experimental setup.** SLM, spatial light modulator; BS, beam splitter; L, lens; FM, Fourier mask; AT,variable attenuator; SBN, strontium barium niobate crystal; CCD, charged-coupled device. Bottom-left, the phase diagram for N = 5; bottom-right, the structure of Fourier mask.